Design and Stabilization of a One Legged Hopping Robot

B.Tech. Project

of

Pratik Chaudhari

Roll No. - 06D01015

under the guidance of

Prof. Hemendra Arya
Department of Aerospace Engineering, IIT Bombay.

and

Prof. Bhartendu Seth
Department of Mechanical Engineering, IIT Bombay.

Indian Institute of Technology Bombay
October 28, 2009

Certificate

This is to certify that this report of **Pratik Chaudhari** on the topic, **Design and Stabilization of a One Legged Hopping Robot** towards the fulfillment of the requirements of **B.Tech. Project AE 497** is approved by me for submission. It represents the work carried out by the student under my guidance.

Prof. Hemendra Arya

Guide

Prof. Bhartendu Seth

Co-guide

Acknowledgment

I wish to express my sincere gratitude to Prof. Seth and Prof. Arya for supporting and guiding me during the entire duration of this seminar.

Contents

Abstract

The abstract goes here.

Keywords:
parameter estimation, lyapunov stability of adaptive laws, adaptive control of MAV, fuzzy adaptive control, dynamically focussed learning, magnetic levitation

List of Figures

Chapter 1

Introduction

This is a test.

Chapter 2

Problem Statement

This is a test.

Chapter 3

Mechanical Design

As pointed out in the previous chapter, the major task of this project was to devise an efficient mechanical design. Two different designs both based on extension springs were looked into. This chapter describes them and the motivation behind choosing the final design to be fabricated.

3.1 Design 1

3.1.1 Energy pumping

Figure 3.1: Winding motor with pulley on the leg

Fig. 3.1 shows the pulley mechanism for storing energy in the large central spring. The winding motor is placed upon the platform which can be called as the larger mass M of the two mass system. A winch connects the motor to the same platform passing over the pulley on the lower leg. Thus, as the motor rotates, it pulls the platform (and itself) downwards while extending the spring above it. A few points to note about the energy pumping design are,

1. The motor has to move a distance twice that of the extension of the spring. This is especially important when we look at the timescales over which we have to extend the spring, these are around 200-300 msecs. A larger distance in smaller time results in a large ω for the motor which translates to a smaller available torque. This neccesitates a larger motor that can provide this torque.
2. The large mass of the platform (M) is helping in the extension of the spring and hence the torque required for the winding motor reduces.
3. It has to be ensured that the winding winch does not slip over the pulley when the platform is suddenly released from the constraint. At the same time, the winch must be free enough so as not to hinder the movement of the platform after the release.

3.1.2 Constraint

Figure 3.2: Constraint for the pulley

Fig. 3.2 shows the constraint mechanism for the pulley. It consists of a hatch connected to the lower leg with a torsional spring. The toothed part of the pulley is free to move in the clockwise direction (thus

compressing the torsional spring every time). The lower part of the leg is cylindrical with a top flange which matches the top face of the cylindrical bushing shown inside the main leg. Thus the lower leg can move only up. The protruding portion of the main leg prevents the hatch from moving in the clockwise direction, thus constraining the pulley from rolling back in the anti-clockwise direction.

- The diameter of the lower leg is expected to be around 2-3 cms and it is difficult to fabricate the hatch on such a small surface.

3.1.3 Using the impact for energy release

This design is unique because it utilizes the impact force ($m\, v_{touch-down}$) to release the stored energy in the main spring. Visualize the lower leg impacting on the ground. This results in the hatch (which is holding the pulley from moving back) impacting against the protrusion of the main leg. Since the impact force is easily larger than the torsional spring force, the hatch closes and the lower leg goes inside the main leg thus enabling free rotation of the pulley. There is a compression spring inside the main leg connected to the lower leg which gets compressed while this happens. It is responsible for pushing the lower leg back outside after $t_{liftoff}$.

3.2 Design 2

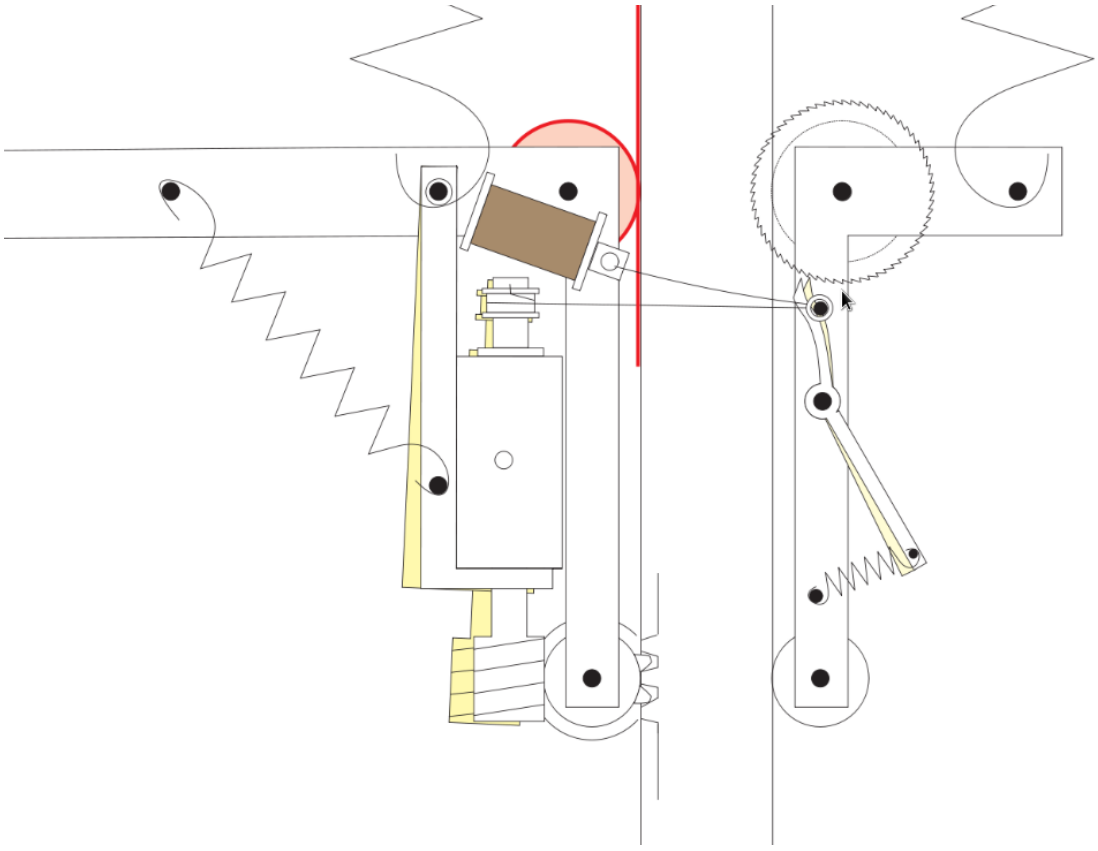

Figure 3.3: Rack and pinion on the leg with the drive motor

3.2.1 Energy pumping

The leg consists of a rack on one of its sides. A single dual shaft motor in a sleeve is used to drive the pinion on this rack as well as pull the paul to free the ratchet. This motor consists of a string attached to a friction pulley on the shaft. A friction pulley is a device whose coupling is dependent upon the speed of the relative motion between the two surfaces. Thus, the motor can pull the paul only beyond a certain ω. Below this speed, the paul spring is strong enough to engage it with the ratchet. After the paul engages, the string becomes slack again.

3.2.2 Constraint

The platform and the ratchet are rigidly connected to a band drive which rolls along the length of the leg. This ensures that contact of the roller inside the band drive and the leg is maintained at all times. Since the ratchet is rigidly connected to the platform, both can only move together i.e. only when the paul is pulled by the drive motor.

3.2.3 Energy release

This design uses an electromechanical system to release energy. After sensing the impact through a touch switch located below the leg, we can use a voice coil actuator to pull the string which in turn moves the paul. This brings in the pull back spring attached to the sleeve into the picture and it prompty pulls the sleeve away from the rack. Note that the string attached to the drive motor pulley is slack at this point.

3.2.4 Evaluation

- The worm-worm wheel on the rack mechanism provides a huge mechanical advantage and thus reduces the maximum torque required from the motor. This scales down the mechanical system as well as the electronic system requirements.
- The friction pulley has to work against the pual spring, sleeve spring and the horizontal component of the rack force ($k\,x\,tan\,\theta$) to keep the string in tension. This is compounded by the fact that the there is a maximum ω the motor can accelerate to in the energy storing phase. It is much better if this ω is dictated by the torque requirements which are as critical rather than this mechanism.

Chapter 4

Sizing of Hardware

This chapter details the sizing of the various components of the design chosen in Chapter 3. The major parts of this process are,

1. Masses of the platform and the leg
2. Dimensions of the reaction wheel based on the above masses
3. Choice of winding and reaction wheel motors

4.1 2 mass problem

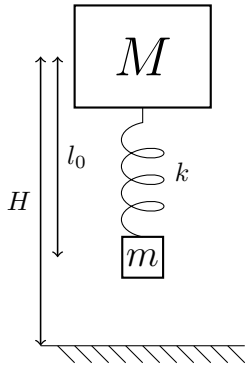

Figure 4.1: 2 mass problem

The basic idea behind a hopper is like that of the 2 masses connected by a spring problem. If the system shown in Fig. 4.1 is allowed to fall from a height, the heavier mass pulls the smaller mass with it back into the air after impact. Every cycle is accompanied by a loss in energy due to the inelastic impact of the smaller mass with the ground. If we pump this energy back into the system using an external agent in every cycle, we can ensure sustained hopping at the chosen height. The 2 mass problem can thus be taken as a basis to compute the range of values of masses for acceptable performance. The following assumptions have been used in the simulation that follows,

1. Dropping height (H) : 0.6 m
2. Spring constant (k) : 300 N/m
3. Spring relaxed length (l_0) : 0.3 m

4. Trapezoidal profile for ω of the winding motor (constant α at the start and end)

5. Faulhabeur 2342CR024 motor with a 3.71 reduction gear-box for comparison of torques

6. Neglect energy loss due to friction

It is seen from Fig. 4.1 that if h_i are progressive heights, we have the relation,

$$h_n = \frac{Mh_{n-1} + ml_0}{M+m} \tag{4.1}$$

$$E_{loss} = \frac{Mg\,(H - l_0)}{1 + M/m} \tag{4.2}$$

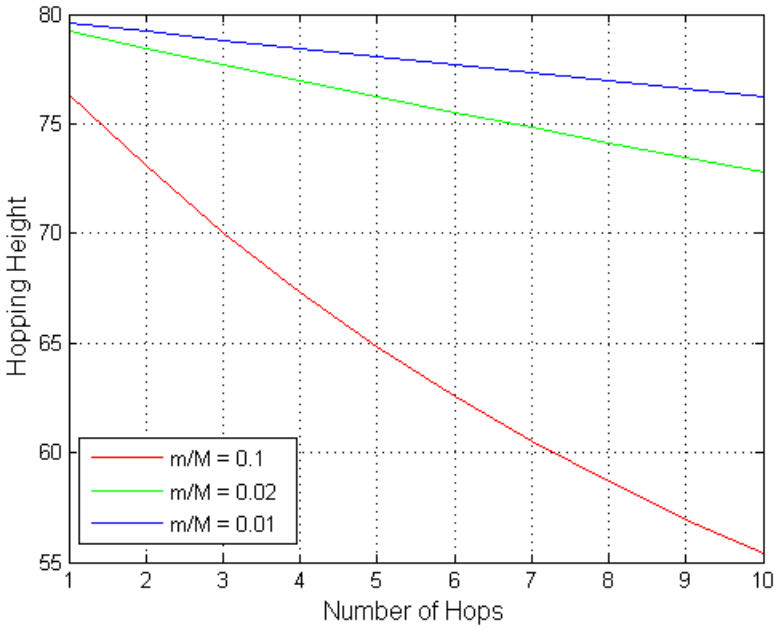

Figure 4.2: Hopping height for different M/m

From Fig. 4.2, it is seen that larger the ratio M/m, i.e. smaller the leg mass, less is the loss in energy resulting in more number of hops. This is also seen for a increasing M. We would however, like the M to be within limit too as we will also need to pump in extra energy into the system if the desired hopping height is more than the starting height.

Figure 4.3: Torque variation with m

Change simulation to take care of torque for a rack and pinion

4.2 Impact analysis

The desired hopping height dictates a hopping frequency. Smaller hopping height results in large number of impacts per time and consequently in larger energy loss per unit time. However, beyond this consideration, since the hopper is a spring mass system, it possesses a natural frequency of its own. If the hopping frequency is near to this natural frequency, a large amount of energy is taken away by impact forces in every cycle. We intend to arrive at a range of values for the masses to ensure a large difference

between the hopping frequency (ω_{hop}) and the natural frequency (ω_{nat}). The details of this analysis are as follows,

- Conserve energy at H and the moment of maximum extension of the spring after $t_{touchdown}$ to get the minimum height of the fully extended platform above the leg. This comes out to be 8 cms for m = 0.4 kg. This value also reduces with increasing m. I assumed no pre-extension of the spring while calculating this. The final value will be less then 8 cms if we take it into account. Thus we say that the leg should protrude about 12 cms beyond the maximum extension of the platform which is obtained from Fig. 4.2.
- If x_2 is the height of C.G. just before touchdown, we can calculate the time taken for it to fall from a height H to x_2 as t_1.
- M undergos simple harmonic motion from time t_1 till liftoff, and this time of motion is t_2
- M transfers its momentum at $t_1 + t_2$ to m resulting in a velocity v_{cg,t_2} for the C.G. To ensure that M has largest velocity while transfering momentum to m, we need to put a mechanical stopper at the natural length of the spring.
- The resultant velocity is just enough for the C.G. to reach a height H in time t_3.
- Total hopping time T = $t_1 + t_2 + t_3$, with $\omega_{hop} = \frac{2\pi}{T}$.
- $\omega_{nat} = \sqrt{\frac{k\ (1+m/M)}{m}}$

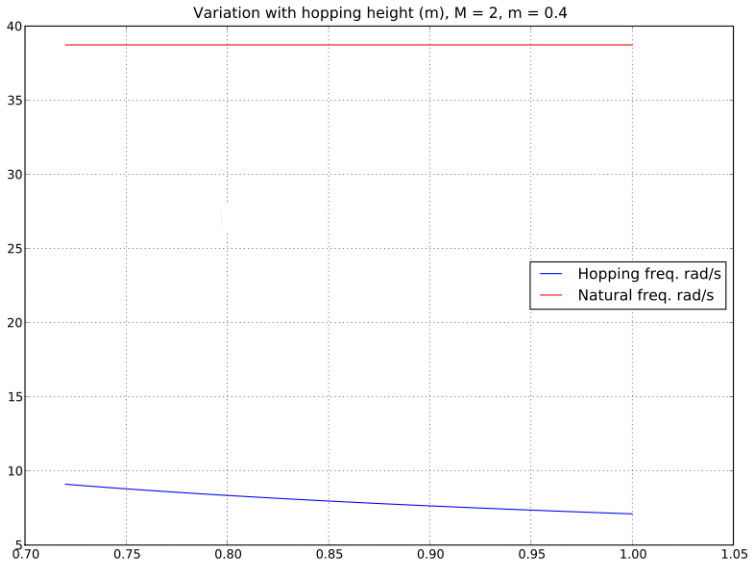

Figure 4.4: Frequency variation with hopping height for M/m = 5

Fig. 4.4 shows that ω_{hop} and ω_{nat} are seperated by large gap for the usable range of values of hopping height. A similar analysis for variation of M also reveals that the two frequencies are seperated by a large gap for all usuable values. Fig. 4.5 succintly depicts all the above analysis. As the leg mass increases, the hopping frequency goes closer to the natural frequency i.e. more impact per unit time. To compound matters, more and more energy is lost per impact as per Eqn. 4.2. So the conclusion from impact analysis is that the leg mass should be as low as possible. It is also seen from Fig. 4.5 that m = 0.4 – 0.6 kg is a good solution as well as an achievable one.

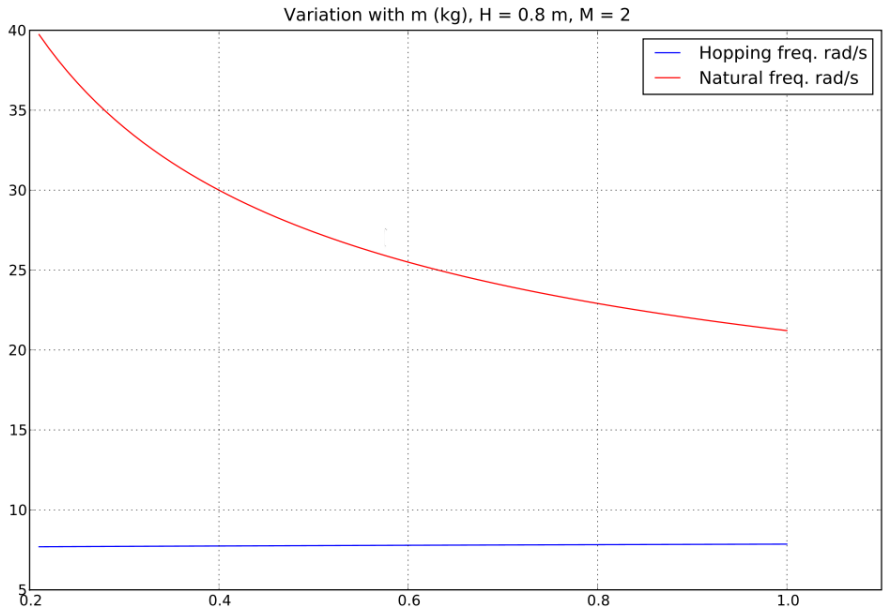

Figure 4.5: Frequency variation with m

4.3 Reaction wheel

For achieving a running gait with the hopper, it has to be started with the exact initial pitch and horizantal velocity. For any other initial condition, the hopper is pitch unstable and will not be able to continue the running gait. As mentioned in (cite shanmukh...), an offset mass acts as a passive stabilization to the pitch attitude of the hopper. To get rid of this need for exact initial condition which is quite impractical, we design a reaction wheel on the hopper. This will result in torque coupling on the pitch axis and thus provide an active control over the pitch of the robot. The coupling equation can be written as,

$$J_{wheel}\ \omega_{wheel} = -(J_{wheel} + J_{body})\ \omega_{body} \tag{4.3}$$

The following considerations are made for this analysis,

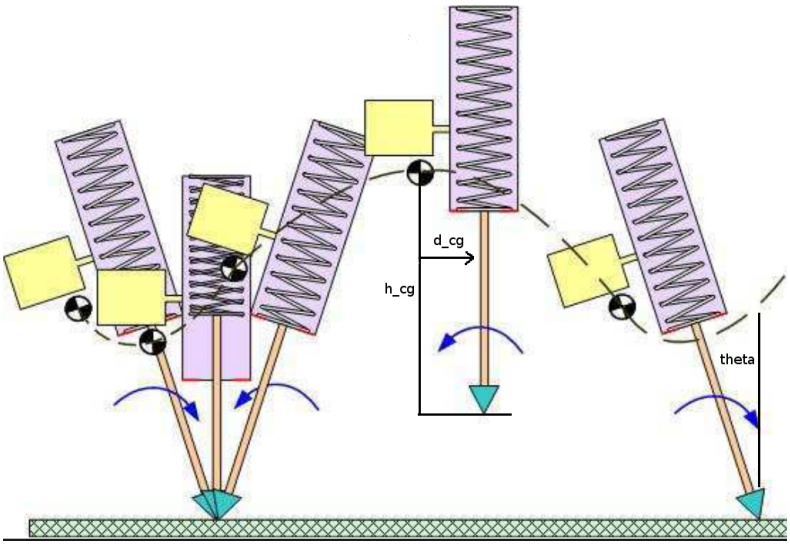

Figure 4.6: Stabilizing impact torque due to SLOM

- The reaction wheel is taken as a ring with mass concentrated at the rim.
- Let θ_{impact} be the impact pitch attitude and $\theta_{liftoff}$ be the lift-off attitude. Pitch is measured with respect to the vertical direction. An upright hopper means a pitch of zero.
- From Fig. 4.6, the stabilizing impact torque is given by $\tau_{impact} = m\, v_{impact}\, (h_{cg} sin\, \theta + d_{cg} cos\, \theta)$. This is positive torque and generates a pitch up. Thus we have a $\omega_{liftoff} = \tau_{impact}\, / J_{body}$
- The angle rotated due to horizantal velocity in the stance phase is $\Delta\, \theta = -v_h\, / h_{cg}\, \Delta\, t$. This means $\theta_{liftoff} = \theta_{impact} + \Delta\, \theta$.
- The lift-off pitch needs to be corrected to θ_{impact} while the hopper is in the air. $\omega_{liftoff}$ might not be enough to correct this pitch and so we need an additional reaction wheel.
- We assume a trapezoidal profile for ω_{wheel} with length of the plateau taken as $0.3\, T_{air}$. The acceleration phase is $0.2\, T_{air}$ on either side. This means that we finish the reorientation task within 7/10 ths of the total time the hopper remains in the air ($T_{air} = t_1 + t_3$ from Section 4.2).

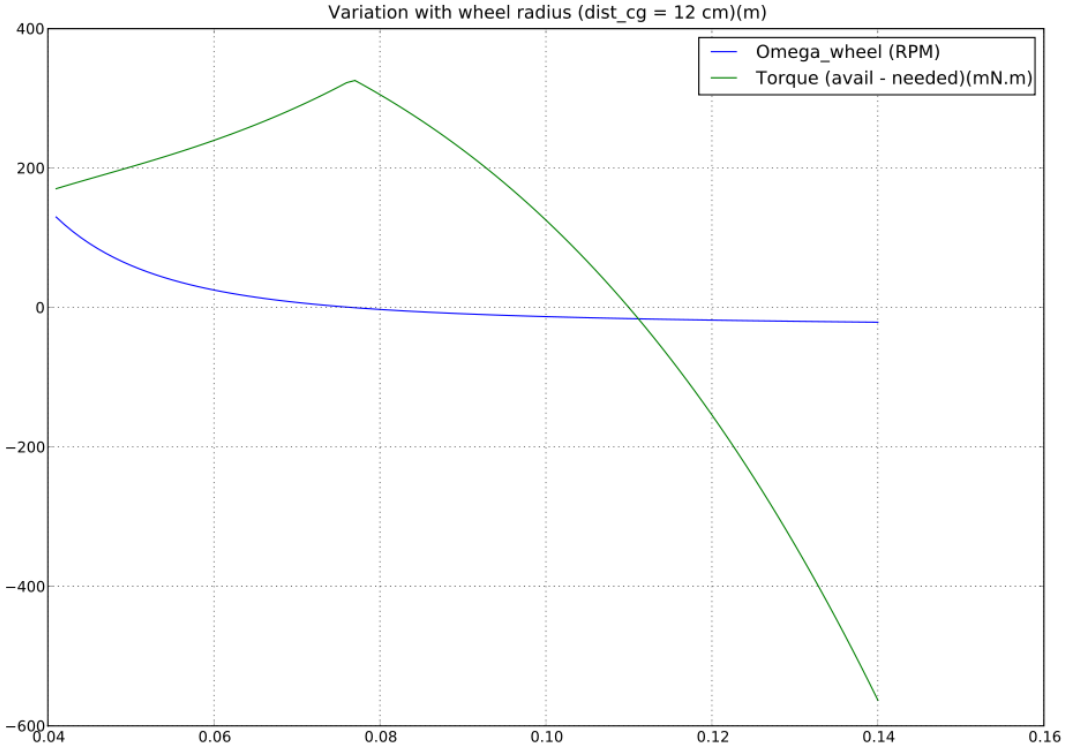

Figure 4.7: Torque requirements vs wheel radius

4.3.1 Results

It is seen from Figs. 4.7 and 4.8 that a reaction wheel radius of 8 cm with a C.G. offset of 12 cms lie near the peak of both the plots. They can be taken as the final values for fabricating the hopper.

4.4 Choosing the Motors

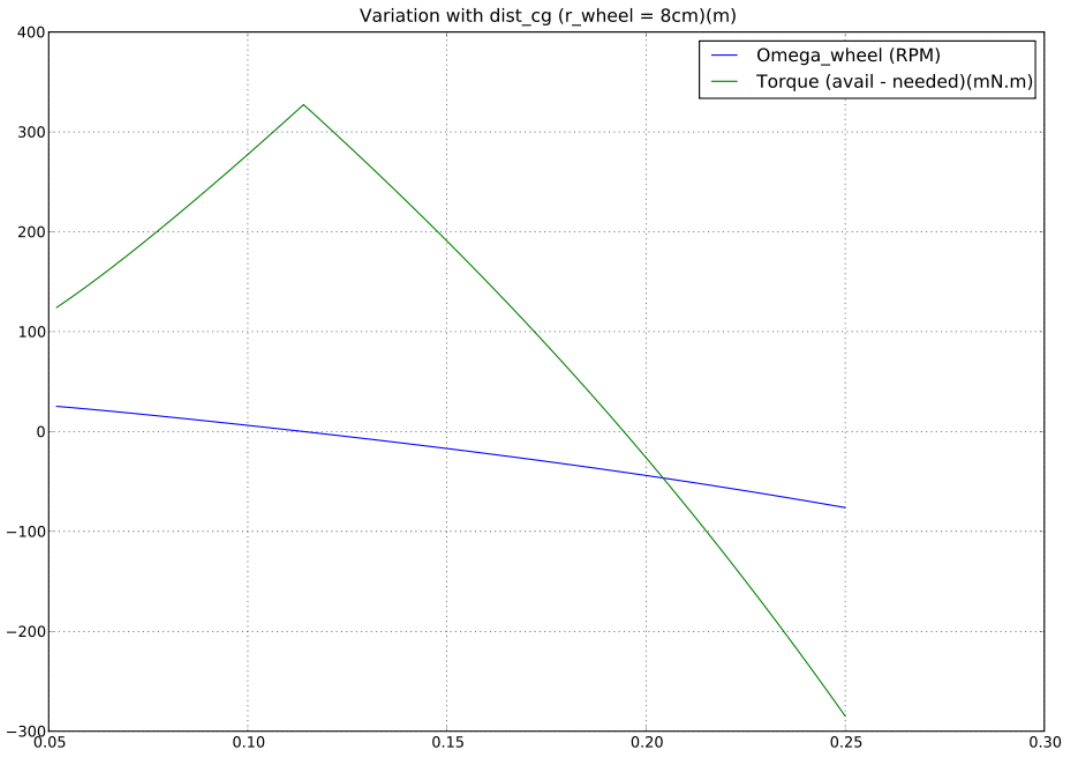

Figure 4.8: Torque requirements vs C.G. offset

Chapter 5

Embedded System

This chapter details the development of the embedded system necessary for controlling and actuating the hopper. It consists of two major parts yet,

1. Micro-controller and RF interface
2. Inertial Measurement Unit (IMU)

5.1 Micro-controller

The microcontroller chosen for this system is a Microchip dsPIC33F64MC804. It can run at 40 MIPS with an onboard flash memory of 64 KB along with a 16 KB SRAM. There are a host of integrated peripherals like Serial Peripheral Interface (SPI), UART, Analog to Digital convertor (ADC), Quadrature Encoder (QEI) and timers to generate Pulse Width Modulation (PWM) that can be used for motor control. Other major features provided with it are the Direct Memory Access controller (DMA) which can transfer memory from one peripheral to other without CPU intervention and the high multiplexing of its IO pins. The latter enables almost all IO pins to be assigned to any of the above mentioned peripherals (except analog pins) and greatly simplifies design. Pickit 2 is a programmer cum debugger that had been ordered for programming the micro-controller.

XBee modules using the Zigbee protocol are used to form a wireless link with the embedded system on the hopper. The range of these devices is quite sufficient for indoor uses (about 100 m). The interface on the microcontroller side is through UART and a custom made FT232 module will be used to interface it with the base station to gather telemetry. A python module to grab and plot this telemetry from the virtual serial port of FT232 is in development.

The current development board contains one motor driver and its adjoining encoder port. The final module will contain two motor drivers and encoder arrangements for the pinion and the reaction wheel motors.

5.2 Inertial Measurement Unit (IMU)

5.2.1 Hardware

We need to read the current pitch of the hopper for proper reorientation before every hop. This is done with the help of an IMU. It consists of a two-axis accelerometer (ADIS 16201) and a single axis gyroscope

(ADIS 16255). Both provide 14-bit signed readings via the SPI interface with internal temperature bias compensation for the gyroscope. Using a digital sensor has benefits over an analog output sensor because the ADC of the micro-controller can give a maximum resolution of only 12 bits as compared to the 14-bit reading given by these sensors.

The sensitivity of the gyroscope is 0.07326^o/sec/LSB for the whole range of $\pm$ $320^o/s$ with excellent noise rate density of $0.056^o/\text{s}\sqrt{Hz}$. The accelerometer has a sensitivity of 2.162 LSB/mg with a noise rate density of $0.37/\text{LSB}/\sqrt{Hz}$. It also consists of an inclinometer to measure the angle with respect to the ground. However, it provides a sensitivity of only 10 LSB/deg. This necessitates the need of onboard inverse tangent tables to get the pitch angle from accelerometer readings. The bandwidth of the gyroscope is 50 Hz as compared to 2.25 kHz of the accelerometer. This severely limits the update rate of the filter and hence we need a better gyroscope.

5.2.2 Kalman Filter

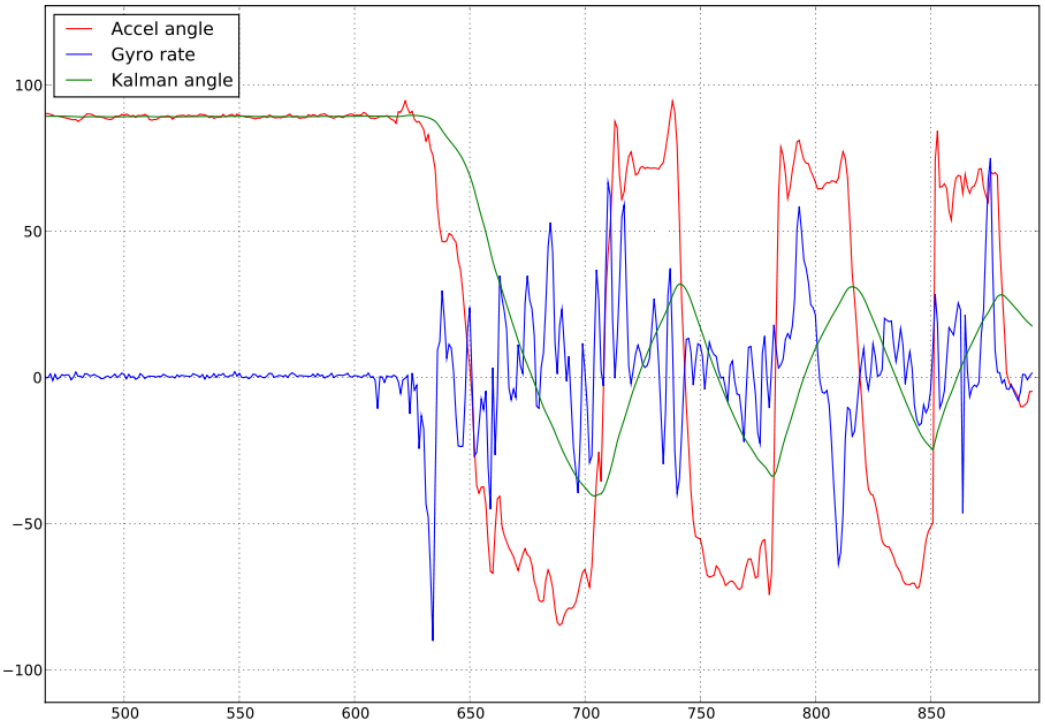

Figure 5.1: Kalman filter for low frequency input

As shown in Fig. 5.1, the readings of the gyroscope and the accelerometer are highly noisy and erratic even in the situation of smooth movements of the IMU. This shows, that depending upon either of the two sensors is not good for pitch estimation. Gyroscopes are high frequency sensors and accurately estimate the rate. However, they also show pronunced variation of readings with time (gyro bias) and temperature (compensated to an extent). Accelerometers are good at low frequency measurements. These do not suffer from a growing bias like the accelerometers can be used to thus correct the readings estimated on the basis of gyroscope angle time to time. We look at Kalman filter as a way to fuse these two sensors.

Various alternatives for filtering schemes exist and complementary filters are very widely used for fusing accelerometers and gyroscopes on IMUs. I decided to use a Kalman filter because the micro-controller

can easily handle the computations at usuable update rates of about 20-50 Hz. This is one of the major reasons cited in literature for the use of complementary filters over Kalman filters (cite 1975 paper). It is also noted that for linear systems, there is little difference in the equations of the two fiters.

The equations for Kalman filter with a state vector $\boldsymbol{x} = [x_1 \;\; x_2]^T = [\theta \;\; \dot{\theta}]^T$ are give below.

State equation :

$$\boldsymbol{x}_{k+1} = \boldsymbol{A}\,\boldsymbol{x}_k + \boldsymbol{B}\,\boldsymbol{u}_k + \boldsymbol{w}_k \tag{5.1}$$

Output equation :

$$y_{k+1} = \boldsymbol{C}\,\boldsymbol{x}_{k+1} + z_{k+1} \tag{5.2}$$

Update equations :

$$\boldsymbol{K}_k = \boldsymbol{A}\,\boldsymbol{P}_k\,\boldsymbol{C}^T\,\left(\boldsymbol{C}\,\boldsymbol{P}_k\,\boldsymbol{C}^T + S_z\right)^{-1} \tag{5.3}$$

$$\hat{\boldsymbol{x}}_{k+1} = (\boldsymbol{A}\,\hat{\boldsymbol{x}}_k + \boldsymbol{B}\,\boldsymbol{u}_k) + \boldsymbol{K}_k\,(y_{k+1} - \boldsymbol{C}\,\hat{\boldsymbol{x}}_k) \tag{5.4}$$

$$\boldsymbol{P}_{k+1} = \boldsymbol{A}\,\boldsymbol{P}_k\,\boldsymbol{A}^T + \boldsymbol{S}_w - \boldsymbol{A}\,\boldsymbol{P}_k\,\boldsymbol{C}^T\,S_z^{-1}\,\boldsymbol{C}\,\boldsymbol{P}_k\,\boldsymbol{A}^T \tag{5.5}$$

For our state vector, the equations consist of,

$$\boldsymbol{A} = \begin{bmatrix} 1 & dt \\ 0 & 1 \end{bmatrix} \quad \boldsymbol{B} = \begin{bmatrix} dt \\ 0 \end{bmatrix} \quad \boldsymbol{u} = \begin{bmatrix} \dot{\theta}_{gyro} \\ 0 \end{bmatrix} \quad y = \theta_{accel} \quad \boldsymbol{C} = \begin{bmatrix} 1 \\ 0 \end{bmatrix} \tag{5.6}$$

$\boldsymbol{P}$ is called the estimation error co-variance and can be initilized to some value, a small value implies that we expect the error co-variance to be around this value. We assume that the estimation errors are completely dependent upon one another and hence initialize the matrix as identity. S_z is the accelerometer variance obtained from the datasheet. $\boldsymbol{S}_w$ is the gyroscope covariance matrix. Let $\nu_{angle} = dt\,\sigma_{rate}$ and $\nu_{rate} = 0$. These values are thus obtained from the datasheet for a particular filter update rate.

$$\boldsymbol{P} = \begin{bmatrix} 1 & 0 \\ 0 & 1 \end{bmatrix} \quad \boldsymbol{S}_w = \begin{bmatrix} \nu_{angle}^2 & \nu_{angle}\,\nu_{rate} \\ \nu_{angle}\,\nu_{rate} & \nu_{rate}^2 \end{bmatrix} \tag{5.7}$$

Eqns. 5.1, 5.2, 5.4 and 5.3 were converted to their algebriac form instead of the matrix operations for better calculation speed. Fig. 5.1 shows the performance of this filter with calculations being done on the computer. Fixed-point arithmetic has been implemented on the micro-controller and will be used for the onboard Kalman filter.

Results

Figure 5.2: Kalman filter for high frequency input

Write the analysis here.

Figure 5.3: Kalman filter : Gyro drift effect

5.3 Motor Control

Chapter 6

Future Work

This is a test.